Transmission Electron Microscopy and High-Resolution Electron Microscopy Study of YNi_2B_2C Thin Film on Y_2O_3-Buffered MgO

G. H. Cao,* P. Simon,† and U. Krämer

Institute of Structural Physics, TU Dresden, D-01062 Dresden, Germany

S. C. Wimbush and B. Holzapfel

IFW Dresden, P.O. Box 270016, D-01171 Dresden, Germany

Received February 26, 2003. Revised Manuscript Received October 27, 2003

An YNi_2B_2C thin film deposited on an Y_2O_3-buffered (001) MgO substrate by pulsed laser deposition has been investigated by X-ray diffraction, transmission electron microscopy (TEM), and high-resolution electron microscopy. Cross-sectional TEM analyses show that the YNi_2B_2C film grows in the [001] direction while the Y_2O_3 buffer layer exhibits columnar growth in the [001] and [111] directions on the (001) MgO substrate, with the growth in the [001] direction being preferred. The orientation relationships of the YNi_2B_2C film, Y_2O_3 buffer layer, and MgO substrate were obtained. The primary orientation relationship YNi_2B_2C-(001)[110] || Y_2O_3(001)[100] || MgO(001)[100], evident from X-ray analyses, was able to be confirmed in the TEM study. A hexagonal impurity phase $Y_{0.915}Ni_{4.12}B$ with lattice parameters $a = 1.491$ nm and $c = 0.692$ nm was identified at the interface between the Y_2O_3 buffer layer and the YNi_2B_2C thin film.

Introduction

Intermetallic compounds of the series RNi_2B_2C (R: rare earth) have aroused great interest due to the interplay of magnetic ordering and superconductivity within the materials. (For a review, see for example ref 1.) Nonmagnetic members of the series (R: Y and Lu) exhibiting fairly high T_c values of 15−16 K are ideal for studying the fundamental superconducting properties of the materials, uninfluenced by magnetic effects.[2] Considerable research has been reported on these compounds in polycrystalline bulk form and in single crystals. On the other hand, high-quality thin films of RNi_2B_2C are of great importance for the performance of several key experiments to understand the nature of the superconductivity in this class of compounds and to explore possible applications. YNi_2B_2C thin films have been prepared by several groups, using both sputtering[3,4] and pulsed laser deposition.[5,6] X-ray diffraction of YNi_2B_2C thin films on MgO repeatedly shows the existence of an Y_2O_3 phase,[4,5] considered to result from the chemical reaction of deposited yttrium with oxygen released from the MgO substrate to produce an interfacial Y_2O_3 layer. As a result of this uncontrolled formation of Y_2O_3, the stoichiometry of the borocarbide is affected, leading to the existence of impurity phases such as Ni_3B and YNi_4B within the films.[7]

To avoid the uncontrolled formation of the Y_2O_3 interfacial layer with the intention of eliminating these impurity phases, in the present work, an Y_2O_3 buffer layer was first deposited on the MgO substrate and the resulting Y_2O_3-buffered MgO then used as a substrate for deposition of YNi_2B_2C. The objectives of this investigation are the fabrication of an epitaxial YNi_2B_2C thin film on the Y_2O_3-buffered MgO, and the characterization of the microstructure of the thin film by transmission electron microscopy (TEM) and high-resolution electron microscopy (HREM). Such a study will expand the synthetic realm of borocarbide thin films, providing a better understanding of their growth processes and the relationship between their microstructure and macroscopic physical properties.

Experimental Section

The Y_2O_3 (206, $Ia3$, $a = 1.0608$ nm) buffer layer was prepared by pulsed laser deposition from elemental yttrium (99.9% purity) onto an (001) MgO (225, $Fm3m$, $a = 0.4212$ nm) substrate held at 700 °C in a 0.5 mbar oxygen atmosphere. The incident energy density on the target was ~3 J·cm^{-2} at a laser pulse repetition rate of 5 Hz. The Y_2O_3-buffered MgO was then used as the substrate in a subsequent process during which an YNi_2B_2C (139, $I4/mmm$, $a = 0.3533$ nm, $c = 1.0566$

* To whom correspondence should be addressed. Tel: +49 351 4633 4749. Fax: +49 351 4633 7048. E-mail: ghcao@physik.tu-dresden.de.

† Current address Max-Planck-Institute for Chemical Physics of Solids, D-01187 Dresden, Germany.

(1) Müller, K.-H.; Narozhnyi, V. N. *Rep. Prog. Phys.* **2001**, *64*, 943.

(2) Häse, K.; Wimbush S. C.; Paschen, S.; Holzapfel, B. *IEEE Trans. Appl. Supercond.* **2001**, *11*, 3836.

(3) Arisawa, S.; Hatano, T.; Hirata, K.; Mochiku, T.; Kitaguchi, H.; Fujii, H.; Kumakura, H.; Kadowaki, K.; Nakamura, K.; Togano, K. *Appl. Phys. Lett.* **1994**, *65*, 1299.

(4) Andreone, A.; Iavarone, M.; Vaglio, R.; Manini, P.; Cogliati, E. *Appl. Phys. Lett.* **1996**, *69*, 118.

(5) Wimbush, S. C.; Häse, K.; Schultz, L.; Holzapfel, B. *J. Phys.: Condens. Matter* **2001**, *13*, L355.

(6) Grassano, G.; Marrè, D.; Pallecchi, I.; Ricci, F.; Siri, A. S.; Ferdeghini, C. *Supercond. Sci. Technol.* **2001**, *14*, 117.

(7) Reibold, M.; Wimbush, S. C.; Holzapfel, B.; Krämer, U. *J. Alloys Compd.* **2002**, *347*, 24.

10.1021/cm031044k CCC: $27.50
Published on Web 01/31/2004

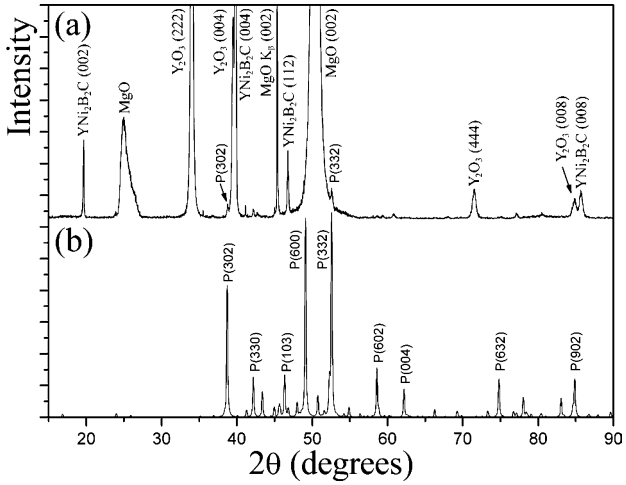

Figure 1. $\theta-2\theta$ X-ray (Co $K\alpha$) diffraction patterns of (a) the YNi_2B_2C/Y_2O_3/MgO sample and (b) an $Y_{0.915}Ni_{4.12}B$ polycrystal (calculated).

nm) thin film was deposited at 750 °C under ultrahigh vacuum, exactly as described in ref 5.

The superconducting transition temperature of the thus fabricated YNi_2B_2C thin film was measured inductively to be 14.2 K, with a transition width of 0.7 K. X-ray diffraction in $\theta-2\theta$ geometry was used to obtain an integral measure of the phases present in the sample. TEM bright-field imaging, electron diffraction, and energy-dispersive X-ray (EDX) analyses of the sample were performed using a Philips CM200Twin electron microscope equipped with a LaB_6 electron source, operated at an acceleration voltage of 200 kV. The HREM images were obtained in a Philips CM200 FEGST-Lorentz electron microscope equipped with a field emission gun, also operated at 200 kV. Cross-sectional samples were prepared by a standard technique involving cutting and then gluing face to face before mechanical grinding and polishing, dimpling, and ion milling to perforation.

Results and Discussion

X-ray Diffraction Analysis of the YNi_2B_2C/Y_2O_3/MgO Sample. The $\theta-2\theta$ X-ray diffraction pattern of the sample is shown in Figure 1(a). The Y_2O_3 buffer layer shows both [001] and [111] oriented growth similar to results previously reported[8,9] for Y_2O_3 films deposited on (001) MgO substrates. The YNi_2B_2C film is predominantly [001] oriented although a weak (112) peak is also visible, suggesting the presence of a small randomly oriented volume fraction. The weaker peaks in Figure 1a, indexed as P(*hkl*), result from an impurity phase of $Y_{0.915}Ni_{4.12}B$, to be discussed in detail below.

TEM and HREM Characterization of the Y_2O_3 Buffer Layer. A bright-field TEM image of the sample is shown in Figure 2a, revealing a sharp interface between the columnar grown Y_2O_3 buffer layer and the MgO substrate. The selected area diffraction pattern (SADP) of the interface (Figure 2b) indicates that the interface region of Y_2O_3 comprises crystallites of differing orientations. Figure 2c is the SADP of a single-crystalline region in the Y_2O_3 buffer layer along the [100] zone axis. Figure 2d is the central dark-field TEM image taken from the (002) spot of Figure 2c, highlighting the [001] oriented grains of the Y_2O_3 buffer layer,

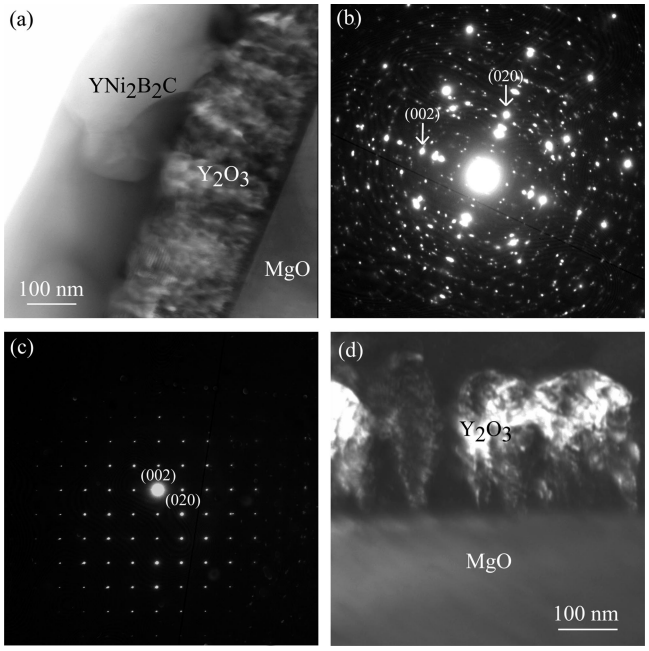

Figure 2. (a) Bright-field TEM image of the sample. (b) SADP of the interface between Y_2O_3 and MgO. Indexed spots (and corresponding spots of higher order) originate from MgO; the others are from Y_2O_3. (c) SADP of a single-crystalline region of Y_2O_3 along the [100] zone axis. (d) Dark-field TEM image taken from the (002) spot of (c), highlighting the [001] oriented grains of Y_2O_3.

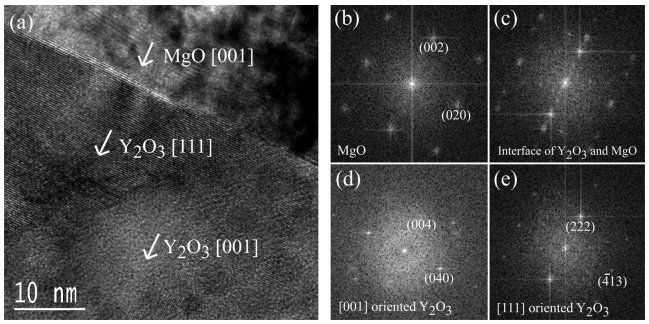

Figure 3. (a) HREM image of the interface region of Y_2O_3 and MgO. Selected area FFTs of (b) MgO, (c) the interface of MgO and Y_2O_3, (d) [001] oriented Y_2O_3, and (e) [111] oriented Y_2O_3.

which are seen to grow preferentially to the exclusion of other, less-preferred orientations.

To determine the in-plane orientation of Y_2O_3 in the buffer layer, HREM imaging of the interface region was carried out with the result shown in Figure 3a. Two distinct Y_2O_3 grains are clearly visible. The fast Fourier transforms (FFTs) of the parts of the image corresponding to each grain, as well as the substrate, and the interface region, are shown in Figure 3b–e. After indexing, it is clear to see that the Y_2O_3 grows with [001] and [111] directions perpendicular to the (001) MgO substrate. Thus, the HREM results are in good agreement with the X-ray diffraction results shown in Figure 1a. The relationships between MgO substrate and Y_2O_3 buffer layer obtained from the FFTs are $Y_2O_3(001)[100]$ || $MgO(001)[100]$ and $Y_2O_3(111)[1\bar{1}0]$ || $MgO(001)[1\bar{1}0]$—the same as those reported previously[7,8] for this system.

TEM Characterization of the YNi_2B_2C Thin Film. Figure 4a is a bright-field TEM image showing the

(8) Gaboriaud, R. J.; Pailloux, F.; Pacaud, J.; Renault, P. O.; Perrière, J.; Huignard, A. *Appl. Phys. A* **2000**, *71*, 675.

(9) Korzenski, M. B.; Lecoeur, P.; Mercey, B.; Chippaux, D.; Raveau, B.; Desfeux, R. *Chem. Mater.* **2000**, *12*, 3139.

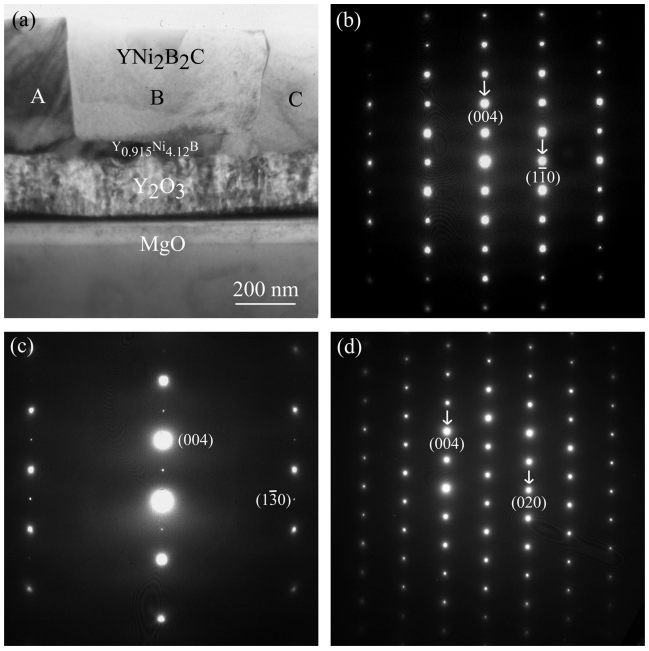

Figure 4. (a) Bright-field TEM image showing differently oriented grains of YNi_2B_2C. SADPs showing YNi_2B_2C along (b) [110] (grain A), (c) [310] (grain B), and (d) [100] (grain C) zone axes.

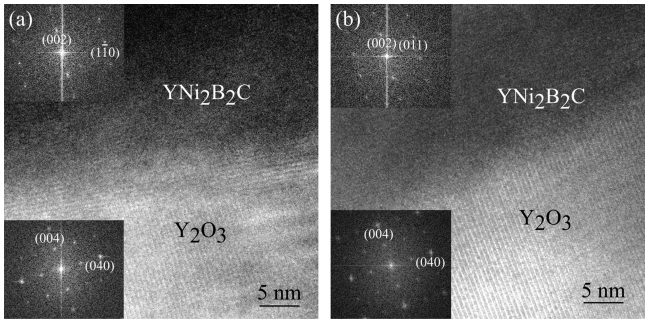

Figure 5. HREM images of the interface region of the Y_2O_3 buffer layer and YNi_2B_2C grains (a) A and (b) C.

YNi_2B_2C film also comprising differently oriented grains. Panels b−d of Figure 4 are the SADPs of these different grains along the [110], [310], and [100] zone axes, showing in each case that the YNi_2B_2C grows [001] oriented (again in agreement with the X-ray results of Figure 1a) but with several different in-plane orientations. Close examination of the TEM image shows that grain B is not growing directly on the Y_2O_3 buffer, but rather upon a grain of another phase (labeled $Y_{0.915}Ni_{4.12}B$), formed at the interface. This phase was then the subject of further investigation, below. Panels a and b of Figure 5 are the HREM images of the interface region of the YNi_2B_2C grains and the Y_2O_3 buffer layer. The orientation relationships between YNi_2B_2C and Y_2O_3 buffer layer obtained from the FFTs for these grains are $YNi_2B_2C(001)[110]$ || $Y_2O_3(001)[100]$ and $YNi_2B_2C(001)[100]$ || $Y_2O_3(001)[100]$. The first of these is consistent with X-ray texture measurements (not shown) performed on this sample, indicating that this is the predominant orientation of YNi_2B_2C. The second in-plane orientation is a common occurrence arising due to the very close lattice match to Y_2O_3 in this orientation.

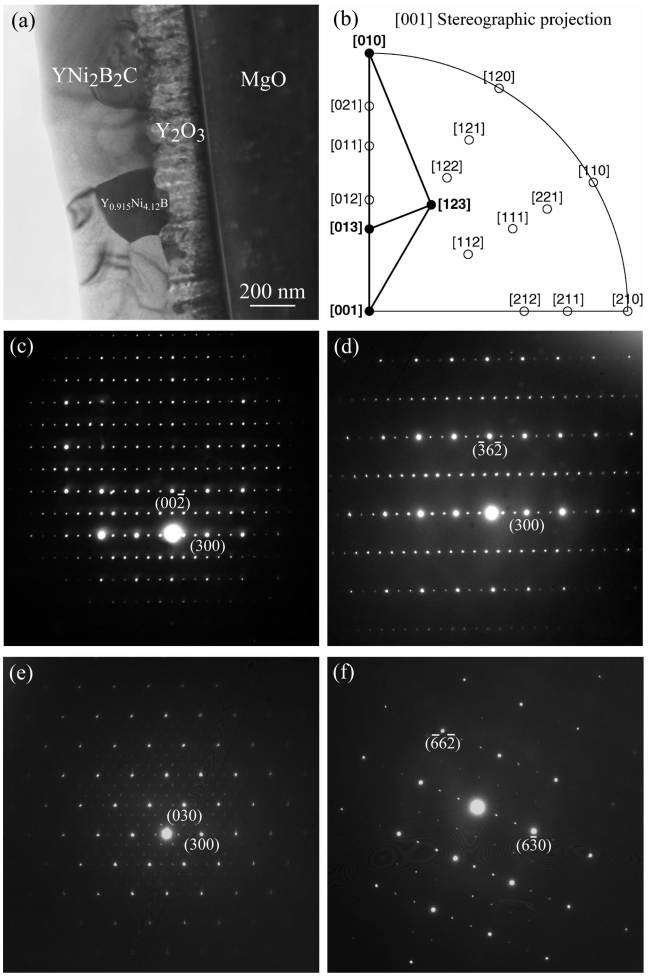

Figure 6. (a) Bright-field TEM image showing a large $Y_{0.915}Ni_{4.12}B$ grain. (b) [001] stereographic projection of $Y_{0.915}Ni_{4.12}B$ showing the rotation route under TEM. SADPs along the (c) [010], (d) [013], (e) [001], and (f) [123] zone axes.

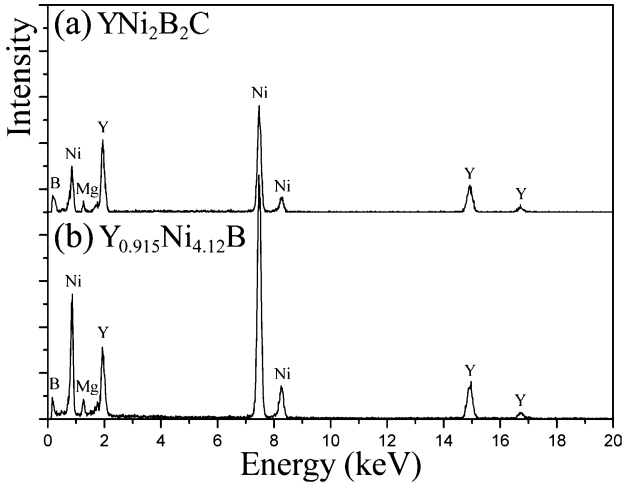

Figure 7. EDX spectra of (a) YNi_2B_2C and (b) the $Y_{0.915}Ni_{4.12}B$ grain of Figure 6.

TEM Characterization of an $Y_{0.915}Ni_{4.12}B$ Impurity Phase. Figure 6a is a bright-field TEM image showing a larger grain of the impurity phase (labeled $Y_{0.915}Ni_{4.12}B$), again found bordering on the Y_2O_3 buffer. EDX analyses were performed (Figure 7), comparing the impurity phase with the YNi_2B_2C phase. The EDX spectrum of the impurity suggests a Ni-rich compound

comprising the elements Ni, Y, and B. (The Mg seen in both spectra originates from the MgO substrate during ion milling.) The Y/Ni ratios, which can be reliably extracted from the scans, lie close to 1:2 for YNi_2B_2C and 1:4 for the impurity. Because the SADP of the impurity grain proved incompatible with the patterns of known compounds such as YNi_4B, the sample was tilted through a wide range of angles (Figure 6b) to obtain SADPs useful in determining its crystal structure. From these patterns (Figure 6c−f), we deduce that it has a hexagonal structure with lattice parameters $a = 1.491$ nm and $c = 0.692$ nm. YNi_4B is one compound in the Y−Ni−B system having a hexagonal structure (191, *P*6/*mmm*), but a much shorter *a* lattice parameter, $a = 0.4977 \pm 0.0004$ nm and $c = 0.6942 \pm 0.0005$ nm.[10] Kuz'ma and Khaburskaya reported[11] that the Y−Ni−B system can form a series of ternary borides, including a hexagonal "YNi_4B" phase with lattice parameters $a = 1.489 \pm 0.005$ nm and $c = 0.691 \pm 0.002$ nm, in agreement with our observation. They considered this YNi_4B to be a superstructure of the other. However, no detailed information such as atomic coordinates is available. Belger et al. reported[12] the full structural information of the phase $Y_{0.915}Ni_{4.12}B$, having matching lattice parameters, also considering this to be a superstructure of YNi_4B.

The calculated X-ray diffraction pattern for $Y_{0.915}Ni_{4.12}B$ is shown in Figure 1b. Comparing this with Figure 1a, it is seen that in the $YNi_2B_2C/Y_2O_3/MgO$ sample the strong peaks P(332) and P(302) of $Y_{0.915}Ni_{4.12}B$ are visible although the P(600) peak is not easily distinguished, possibly due to overlapping by the strong substrate peak. Therefore, based on the crystal structure, lattice parameters, and chemical composition analysis of the impurity phase, we conclude it to be $Y_{0.915}Ni_{4.12}B$. The weak X-ray diffraction peaks resulting from $Y_{0.915}Ni_{4.12}B$ indicate a very low volume fraction of $Y_{0.915}Ni_{4.12}B$ in the sample. That this phase was always found bordering on the Y_2O_3 buffer is an indication that it results from the same process that leads to larger amounts of impurity phases in films without buffer layers, i.e., reaction of deposited yttrium to form Y_2O_3, leading to a deficit of yttrium and resultant formation of Ni-rich phases. Figure 8a is the HREM image of the intersection region of $Y_{0.915}Ni_{4.12}B$, YNi_2B_2C, and Y_2O_3 buffer layer. The FFTs of the parts of the image corresponding to each individual grain are shown in Figure 8b−e. These indicate that there is no well-defined orientation relationship of the $Y_{0.915}Ni_{4.12}B$ to either the Y_2O_3 buffer layer or the YNi_2B_2C film.

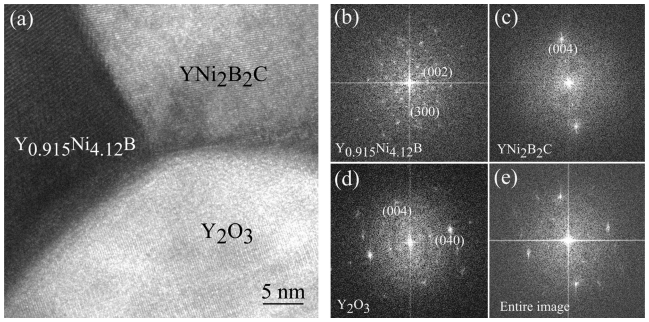

Figure 8. (a) HREM image of the intersection region of $Y_{0.915}Ni_{4.12}B$, YNi_2B_2C, and Y_2O_3. FFTs of (b) $Y_{0.915}Ni_{4.12}B$, (c) YNi_2B_2C, (d) Y_2O_3, and (e) the entire image.

Conclusions

YNi_2B_2C thin films deposited on Y_2O_3-buffered (001) MgO substrates were successfully fabricated by pulsed laser deposition. In this manner, it proved possible to greatly reduce the volume fraction of impurity phases formed during deposition. TEM and HREM investigations of the cross-sectional $YNi_2B_2C/Y_2O_3/MgO$ sample indicate that YNi_2B_2C grows in the [001] direction, while the Y_2O_3 buffer layer exhibits columnar growth in both [001] and [111] directions, with the [001] growth appearing to be preferred. The Y_2O_3 buffer layer and MgO substrate have the orientation relationships $Y_2O_3(001)[100] \parallel MgO(001)[100]$ and $Y_2O_3(111)[1\bar{1}0] \parallel MgO(001)[1\bar{1}0]$, while the YNi_2B_2C film and Y_2O_3 buffer layer have the orientation relationships $YNi_2B_2C(001)[110] \parallel Y_2O_3(001)[100]$ and $YNi_2B_2C(001)[100] \parallel Y_2O_3(001)[100]$. Taking into account the preferential growth of the [001] oriented Y_2O_3, and the predominance of one particular in-plane orientation of YNi_2B_2C observed in X-ray, the sample as a whole can best be described by the orientation relationship $YNi_2B_2C(001)[110] \parallel Y_2O_3(001)[100] \parallel MgO(001)[100]$. A small remaining volume fraction of the hexagonal impurity phase $Y_{0.915}Ni_{4.12}B$ having lattice parameters $a = 1.491$ nm and $c = 0.692$ nm has been identified by TEM analysis.

Acknowledgment. This work was supported by the *Deutsche Forschungsgemeinschaft* as part of SFB463, "Rare earth transition metal compounds: structure, magnetism and transport". The authors thank H. Müller for preparation of the samples for TEM. Helpful discussions with A. Belger are gratefully acknowledged.

CM031044K

(10) Niihara, K.; Katayama, Y.; Yajima, S. *Chem. Lett.* **1973**, 613.
(11) Kuz'ma, Y. B.; Khaburskaya, M. P. *Inorg. Mater.* **1975**, *11*, 1625.
(12) Belger, A.; Zahn, G.; Wehner, B.; Paufler, P.; Graw, G.; Behr, G. *J. Alloys Compd.* **1999**, *283*, 26.